

Decentralized Distributed Learning with Privacy-Preserving Data Synthesis

M. Pennisi, F. Proietto Salanitri, G. Bellitto, B. Casella, M. Aldinucci, S. Palazzo, C. Spampinato

Abstract—In the medical field, multi-center collaborations are often sought to yield more generalizable findings by leveraging the heterogeneity of patient and clinical data. However, recent privacy regulations hinder the possibility to share data, and consequently, to come up with machine learning-based solutions that support diagnosis and prognosis. Federated learning (FL) aims at sidestepping this limitation by bringing AI-based solutions to data owners and only sharing local AI models, or parts thereof, that need then to be aggregated. However, most of the existing federated learning solutions are still at their infancy and show several shortcomings, from the lack of a reliable and effective aggregation scheme able to retain the knowledge learned locally to weak privacy preservation as real data may be reconstructed from model updates. Furthermore, the majority of these approaches, especially those dealing with medical data, relies on a centralized distributed learning strategy that poses robustness, scalability and trust issues. In this paper we present a decentralized distributed method that, exploiting concepts from experience replay and generative adversarial research, effectively integrates features from local nodes, providing models able to generalize across multiple datasets while maintaining privacy. The proposed approach is tested on two tasks — tuberculosis and melanoma classification — using multiple datasets in order to simulate realistic *non-i.i.d.* data scenarios. Results show that our approach achieves performance comparable to both standard (non-federated) learning and federated methods in their centralized (thus, more favourable) formulation.

Index Terms—Decentralized Learning, Federated Learning, Privacy in Machine Learning, Pattern recognition and classification

I. INTRODUCTION

Recent advances of deep learning in the medical imaging domain have shown that, while data-driven approaches represent a powerful and promising tool for supporting physicians' decisions, the availability of large-scale datasets plays a key role in the effectiveness and reliability of the resulting models [1]–[3]. However, the curation of large medical imaging datasets is a complex task: data collection at single

institutions is relatively slow and the integration of historical data may require significant efforts to deal with different data formats, storage modalities and acquisition devices; moreover, medical institutions are often reluctant to share their own data, due to privacy concerns. As a consequence, this affects the quality, reliability and generalizability of models trained on local datasets, which unavoidably suffer from bias and overfitting issues [4]. In order to overcome the lack of large-scale datasets, methodological solutions can be adopted: in particular, federated learning [5] encompasses a family of strategies for distributed training over multiple nodes, each with its own private dataset, which typically communicate with a central node by sending local model updates, used to train the main model. In this scenario, no data is explicitly shared between nodes, thus addressing the required privacy issues. However, this family of techniques generally performs well when dataset distributions are approximately *i.i.d.* and local gradients/models contribute to learning shared features: unfortunately, in practice this hypothesis rarely holds, due to differences in the acquisition and in the clinical nature of data collected by multiple institutions. Moreover, the presence of a central node, besides representing a single point of failure, requires that all nodes trust it to correctly and fairly treat updates from all sources: indeed, privacy issues arise when transferring local updates to the “semi-honest” central node [6], which might attempt to reconstruct original inputs from gradients or parameter variations [7]–[9].

In this work, we propose a decentralized distributed learning approach that combines principles of experience replay [10]–[13] and generative models [14]–[16] to train local independent models that approximately converge to the same solution, while enforcing privacy preservation through the transmission of synthetic data built in a way to obfuscate real data patterns. Specifically, the distributed training procedure envisages multiple nodes that initially train their local models on their own datasets, in order to generate a privacy-preserving synthesized version thereof. Once local training is completed in a node, its model and a “buffer” of generated synthetic data are randomly sent to another node of the network. The receiving node then adapts the incoming model using its own data and the buffer data, in order to limit model's forgetting. Data privacy is ensured through a privacy-preserving generative adversarial network (GAN) that employs a specific loss designed to maximize the distance from real data, while keeping a high level of realism and — as importantly — clinically-consistent features, in order to allow models to be still trained effectively.

M. Pennisi, F. Proietto Salanitri, G. Bellitto, S. Palazzo, C. Spampinato are with the Department of Electrical, Electronics and Computer Engineering, University of Catania, Italy (email: matteopennisi98@gmail.com, federica.proiettosalanitri@phd.unict.it, giovanni.bellitto@phd.unict.it, simone.palazzo@unict.it, concetto.spampinato@unict.it)

B. Casella and M. Aldinucci are with the Department of Computer Science, University of Turin, Italy (email: name.surname@unito.it) Equal contribution by M. Pennisi and F. Proietto Salanitri. Equal supervision by S. Palazzo and C. Spampinato.

Our approach is tested on two tasks, each simulating both *i.i.d.* and *non-i.i.d.* scenarios: 1) classification of tuberculosis with X-ray data, using Montgomery County X-ray and Shenzhen Hospital X-ray sets [17]–[19], and 2) melanoma classification using skin images of the ISIC 2019 dataset [20]–[22]. Results show how our approach is able to reach performance similar to using all real data together in a single node. Privacy-preserving capabilities are measured quantitatively by evaluating LPIPS distance [23] between real images and samples generated, respectively, through latent space optimization on a standard GAN and by the proposed approach. Qualitatively, we also show several examples of generated images with corresponding closest match in the real dataset, demonstrating significant differences that prevent tracing back to the original real distribution.

In summary, the overall contributions of the proposed work are the following:

- We propose, for the first time, a decentralized distributed learning strategy designed for medical imaging data, which performs at least on par with centralized learning approaches and yields performance similar to standard (non-federated) training settings in low-data availability scenarios;
- The distributed learning strategy is model and dataset-agnostic;
- We also propose a privacy-preserving mechanism that supports synthetic data sharing through a GAN-based technique designed to minimize patient information leak;
- We demonstrate that distributing the learning at the data level is an effective, secure and scalable solution to create models able to generalize across multiple datasets while keeping local data private.

II. RELATED WORK

Data scarcity in the medical domain often calls for multi-institutional collaborations, in order to collect enough evidence to draw statistically-significant conclusions, as well as to create automated analysis methods (based on machine learning) to support decision making. However, due to the privacy-sensitive nature of medical information, data cannot be shared, hindering the possibility to create robust learning methods able to effectively support physicians in their clinical routines. Federated Learning (FL) [24] has recently emerged as a family of distributed learning strategies that allow nodes to keep training data private, while supporting the creation of a shared model. In a typical FL setting, a central server sends a model to a set of client nodes; each node fine-tunes the model on its own data, then sends local model updates back to the server; the server aggregates the updates by all nodes into the global model, which is sent back to nodes iteratively until convergence. Given the constraints existing in the medical domain, especially in terms of data sharing, it represents an appropriate test bench for federated learning methods [25]–[29]. The most straightforward way to aggregate information from multiple nodes is through averaging local gradients of each client, as proposed in FedAvg [24]. FedProx [30] demonstrates theoretical convergence guarantee of FedAvg

when training over statistically-heterogeneous (*non-i.i.d.*) data. Statistical data heterogeneity is particularly challenging as it leads to catastrophic forgetting in FL settings [31], [32]. FedCurv [33] addresses this issue by adding a penalty term to the loss function in order to drive the local models to a shared optimum. FedMA [34] builds a shared global model in a layer-wise manner by matching and averaging hidden elements with similar feature extraction signatures. Our method differs from existing feature integration approaches in that, instead of averaging model updates or gradients, which can be subject to input reconstruction attacks [7], [8], [35], each node attempts to learn features that perform well on both its own dataset and other nodes', in a more principled way than crude parameter averaging.

Another novelty of the current work w.r.t. the existing state of the art in the medical domain lies in the network topology. Unlike most solutions in medical federated learning, our strategy is decentralized, i.e., nodes directly exchange information among themselves. Indeed, the presence of a central node that aggregates local updates simplifies the communication protocols when the number of clients is very large (thousands or millions), but introduces several downsides: it represents a single point of failure; it can become a bottleneck when the number of clients increases [36]; in general, it may not always be available or desirable in collaborative learning scenarios [31], [37]. In decentralized learning, the central node is replaced by peer-to-peer communication between clients: there is no longer a global shared model as in standard FL, but the communication protocol is designed so that all local models approximately converge to the same solution. Decentralized distributed learning is particularly suitable to application in the medical domain, where the number of nodes (i.e., institutions) is relatively low; however, research is still ongoing, and no effective solutions have emerged. In [38], a Bayesian approach is proposed to learn a shared model over a graph of nodes, by aggregating information from local observational data with the model of each node's one-hop neighbors. A secure weight averaging algorithm is proposed in [39], where model parameters are not shared between nodes, but all converge to the same numerical values (with the disadvantages associated to parameter averaging with *non-i.i.d.* data distributions). Other approaches implement different communication strategies based on parameter sharing (e.g., gossip algorithms [37] or decentralized variants on FedAvg [24], [40]). In general, most of the existing solutions do not target, nor are they tested on, the medical domains — most employ toy datasets, such as MNIST and CIFAR10. A work which is similar in spirit to ours is BrainTorrent [26], where a use case of decentralized learning for MRI brain segmentation is presented. However, like other approaches, simple parameter averaging is used to integrate features from multiple nodes.

Finally, a key component in our approach lies in the use of generative adversarial networks (GAN) to synthesize samples that can be shared between nodes in a privacy-preserving way. Among similar approaches proposed in the literature, GS-WGAN [41] proposes a gradient-sanitized Wasserstein GAN to improve differential privacy, by carefully distorting gradient information in a way that reduces loss of infor-

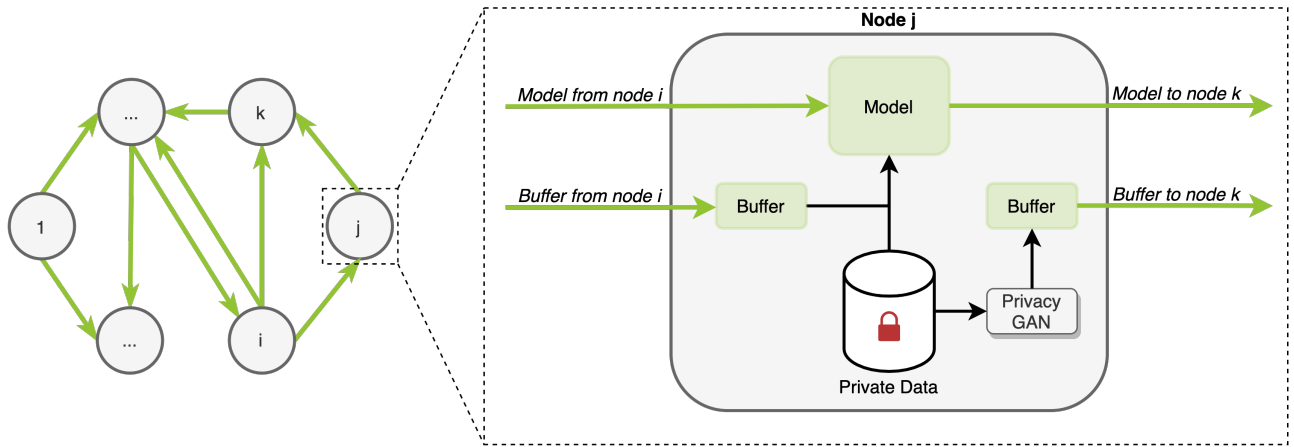


Fig. 1. Overview of the proposed architecture. Each node initially trains a *privacy-preserving GAN*, that is used to sample synthetic data from the local distribution, without retaining features that may be used to identify patients. Then, each node iteratively receives the local model and a buffer of synthetic samples from a random node, and fine-tunes the received model on its own private data, using the buffer to prevent forgetting of previously-learned features.

mation and generates more informative samples. Federated CycleGAN [42] is designed to perform unsupervised federated image translation. FedDPGAN [43] designs a distributed DPGAN [35] trained in a FL framework, to generate models for COVID-19 diagnosis from chest X-ray images, without data sharing. While CycleGAN, GS-WGAN and FedGPGAN share either gradient or model updates of the generator with the server, introducing privacy concerns related to the risk of input reconstruction, in our approach nodes share a subset of synthetic images, generated in a way that discourages privacy-sensitive information leaking, to be used with an experience replay mechanism and enhance feature reuse among nodes.

III. METHOD

A. Overview

An overview of the proposed decentralized distributed learning approach is shown in Fig. 1. In this scenario, a *federation* consists of a set of N peer nodes, each owning a private dataset.

Before the distributed training algorithm is started, each node internally trains a *Privacy-Preserving Generative Adversarial Network*, which is used to generate synthetic samples from the private data distribution. The training objective of the GAN is designed to enforce the constraint that sampled data do not include privacy-sensitive, while maintaining the clinical features required for successful training.

At each round of distributed training, each node receives the current model and a set of synthetic samples — “buffer” — from a randomly-chosen predecessor node, and sends its own model and buffer to a randomly-chosen successor node. The input model is then fine-tuned on both the private dataset and the buffer, in a way that is reminiscent of experience replay techniques in continual learning (e.g., [13]), in order to learn features that transfer between nodes and that can handle *non-i.i.d.* distributions. At the end of the current round (i.e., after performing several training iterations), the locally-trained model is sent to a randomly-chosen successor node, and the whole procedure is repeated.

In this work we specifically address the problem of federated learning for medical image classification; thus, the method is presented by considering this task, but the whole strategy can be applied to any other task without losing generalization.

B. Privacy-preserving GAN

In the proposed method, nodes exchange both models and data, implementing a knowledge transfer procedure based on experience replay (see Sect. III-C below). Of course, sharing real samples would go against federated learning policies; hence, exchanged samples are generated so that they are representative of the local data, while taking precautions against privacy violations — which may happen, for instance, if the generative model overfits the source dataset.

Formally, we assume that each node n_i owns a private dataset $\mathcal{D}_i = \{(\mathbf{x}_1, \mathbf{y}_1), (\mathbf{x}_2, \mathbf{y}_2), \dots, (\mathbf{x}_M, \mathbf{y}_M)\}$, where each $\mathbf{x}_j \in \mathcal{X}$ represents a sample in the dataset, and each $\mathbf{y}_j \in \mathcal{Y}$ represents the corresponding target¹. The local dataset can then be used to train a conditional GAN [15], consisting of a generator G , that synthesizes samples for a given label by modeling $P(\mathbf{x}|\mathbf{y}, \mathbf{z})$, where $\mathbf{z} \in \mathcal{Z}$ is a random vector sampled from the generation latent space, and a discriminator D , which outputs the probability of an input sample being real, modeling $P(\text{real}|\mathbf{x}, \mathbf{y})$. The standard GAN formulation introduces a discrimination loss, which trains D to distinguish between real and synthetic samples:

$$\mathcal{L}_D = -\mathbb{E}_{\mathbf{x}, \mathbf{y}} [\log(D(\mathbf{x}, \mathbf{y}))] - \mathbb{E}_{\mathbf{z}, \mathbf{y}} [\log(1 - D(G(\mathbf{z}, \mathbf{y}), \mathbf{y}))], \quad (1)$$

and a generation loss, which trains G to synthesize samples that appear realistic to the discriminator:

$$\mathcal{L}_G = -\mathbb{E}_{\mathbf{z}, \mathbf{y}} [D(G(\mathbf{z}, \mathbf{y}), \mathbf{y})]. \quad (2)$$

While it has been theoretically proven that, at convergence, the distribution learned by the generator matches and generalizes from the original data distribution [32], unfortunately

¹The proposed approach is task-agnostic, as long as it is possible to sample from the \mathcal{Y} distribution. For simplicity, within the scope of this work, we will focus on classification tasks, and we will assume that targets are class labels.

GAN architectures may be subject to training anomalies, including mode collapse and overfitting: as a consequence, the basic GAN formulation may lead to the generation of samples that are near duplicates of the original samples, which would be unacceptable in a federated learning scenario.

In order to mitigate this risk, we introduce a *privacy-preserving loss*, enforcing the generation of samples that do not retain potentially identifying information, but still include features that are clinically relevant to the target \mathbf{y} of the synthetic sample. In other words, if \mathbf{y} encodes the diagnosis of a certain disease, we want the generator to learn how to synthesize samples conditioned by \mathbf{y} , that exhibit evidence of that disease but cannot be traced back to any of the dataset's samples of the same disease.

To do so, our privacy-preserving loss aims at penalizing the model proportionally to the similarity between pairs of real and synthetic samples. We measure “similarity” by means of the LPIPS metric [23], which has been shown to capture perceptual similarity better than traditional metrics (e.g., SSIM) by calibrating the distance between feature vectors extracted from a pre-trained VGG model [44].

In practice, given a batch of real samples $\{\mathbf{x}_1^{(r)}, \mathbf{x}_2^{(r)}, \dots, \mathbf{x}_b^{(r)}\}$ and a batch of synthetic samples $\{\mathbf{x}_1^{(s)}, \mathbf{x}_2^{(s)}, \dots, \mathbf{x}_b^{(s)}\}$, the privacy-preserving loss term is computed as:

$$\mathcal{L}_{\text{PP}} = \frac{1}{b} \sum_{\mathbf{x}^{(r)}} \sum_{\mathbf{x}^{(s)}} d_L(\mathbf{x}^{(r)}, \mathbf{x}^{(s)}), \quad (3)$$

where d_L is the LPIPS distance. Note that, in this formulation, we ignore the \mathbf{y} targets associated to each \mathbf{x} : we want to prevent the model from generating near-duplicates of real samples in general, regardless of class correspondence. Also, we intentionally employ a pairwise metric on samples, rather than an aggregated metric such as Fréchet Inception Distance [45], since we want to prevent similarity between samples, not between distributions, which would conflict with the GAN objective. The combined effect of the three loss terms — \mathcal{L}_D , \mathcal{L}_G , \mathcal{L}_{PP} — pushes the generator to explore the sample space to match the dataset distribution, while “avoiding” latent space mappings that would project to actual real samples.

C. Decentralized learning with experience replay

Current approaches for federated learning are mostly based on parameter averaging (e.g., FedAvg), which is however a very crude way to combine knowledge from multiple sources: feature locations are not aligned over different models and may be disrupted by updates, before slowly converging to consensus: hypothetically, two models could learn the same set of features at different locations of the same layer, to only have them cancel each other when averaging. In a decentralized scenario, this issue is even exacerbated, due to the lack of an entity that enforces global agreement on node features. In our approach, we address the problem by taking inspiration from continual learning principles [46], where it is necessary to learn how to perform a task without forgetting a previously-learned one: as a consequence, models are encouraged to reuse

and adapt features so that they can equally serve the current and previous tasks.

Given these premises, we define a decentralized learning scenario where a node receives another node's model and surrogate data (generated through the privacy-preserving GAN, since original data cannot be shared) — the “*previous task*” — and fine-tunes that model on its own private data — the “*current task*” — while using received data as a reference to what is necessary to retain/adapt from the knowledge learned by the previous node.

In the following, we describe our method from the point of view of a single node, n_i , which receives information from a predecessor node n_{i-1} . Note that, for a given n_i , the predecessor node n_{i-1} is not fixed: in a practical asynchronous implementation, a node may receive a model and buffer from any random node in the federation at any time, using queues to handle incoming data.

As above, the local dataset at node n_i is $\mathcal{D}_i = \{(\mathbf{x}_1^{(d)}, \mathbf{y}_1^{(d)}), (\mathbf{x}_2^{(d)}, \mathbf{y}_2^{(d)}), \dots, (\mathbf{x}_M^{(d)}, \mathbf{y}_M^{(d)})\}$, while f_θ and $\mathcal{B}_i = \{(\mathbf{x}_1^{(b)}, \mathbf{y}_1^{(b)}), (\mathbf{x}_2^{(b)}, \mathbf{y}_2^{(b)}), \dots, (\mathbf{x}_B^{(b)}, \mathbf{y}_B^{(b)})\}$ are, respectively, the model (with parameters θ) and buffer received from node n_{i-1} . During a round of the learning algorithm, node n_i performs several training iterations on both \mathcal{D}_i and \mathcal{B}_i , using the latter to prevent forgetting of previously-learned features, according to the experience replay strategy [13], [47]. Formally, the training loss is defined as:

$$\mathcal{L}_{n_i} = \mathbb{E}_{\substack{\mathbf{x}^{(d)}, \mathbf{y}^{(d)} \\ \mathbf{x}^{(b)}, \mathbf{y}^{(b)}}} \left[L(f_\theta(\mathbf{x}^{(d)}), \mathbf{y}^{(d)}) + L(f_\theta(\mathbf{x}^{(b)}), \mathbf{y}^{(b)}) \right], \quad (4)$$

where L is the task-specific loss function (e.g., cross-entropy for classification).

After optimizing the \mathcal{L}_{n_i} objective through mini-batch gradient descent for a certain number of training iterations, the resulting model $f_{\theta'}$, with updated parameters θ' , is sent to a random node of the federation, along with a buffer of locally-generated synthetic samples. The number of training iterations and the size of the buffer is discussed in the next section.

Unlike other distributed learning approaches, each node does not have its own local model: as the distributed learning algorithm proceeds, a node iteratively receives a model from another node and updates it with local information, while preserving previously-learned knowledge, before sending it to the next node. As experimentally shown in the next section, at the end of this procedure all models approximately converge to a solution that performs similarly on all private datasets in the federation.

IV. EXPERIMENTAL RESULTS

We test our federated learning approach on two applications: 1) tuberculosis classification from X-ray images, and 2) skin lesion classification. In this section we present the employed benchmarks, the training procedure and report the obtained results to demonstrate the advantages of the proposed approach w.r.t. the state of the art.

A. Datasets

X-ray image datasets for tuberculosis classification. We employ the Montgomery County X-ray Set and the Shenzhen Hospital X-ray Set [17]–[19]. The Montgomery Set contains 138 frontal chest X-ray images (80 negatives and 58 positives), captured with a Eureka stationary machine (CR) at 4020×4892 or 4892×4020 pixel resolution. The Shenzhen dataset was collected using a Philips DR Digital Diagnostic system. It includes 662 frontal chest X-ray images (326 negatives and 336 positives), with a variable resolution of approximately 3000×3000 pixels.

Skin lesion classification. We employ the “ISIC 2019” dataset, which contains 25,331 skin images belonging to nine different diagnostic categories. The data provided belongs to three different sources: 1) the BCN20000 [20] dataset, consisting of 19,424 images of skin lesions captured from 2010 to 2016 in the Hospital Clínic in Barcelona; 2) the HAM10000 dataset [21], which contains 10,015 skin images collected over a period of 20 years from two different sites, the Department of Dermatology at the Medical University of Vienna, Austria, and the skin cancer practice of Cliff Rosendahl in Queensland, Australia; 3) the MSK4 [22] dataset, which is anonymous and includes 819 samples. Among all skin lesion classes, we only consider the melanoma class, posing the problem as a binary classification task.

In our federated learning framework, we consider two settings:

- *non-i.i.d. setting*, the most realistic one, where each dataset is associated to a single node: i.e., two nodes for tuberculosis classification (one with the Montgomery County X-ray Set and the other with the Shenzhen Hospital X-ray set); three nodes for melanoma classification (one with the BCN20000 dataset, one with the HAM10000 dataset and the last one with the MSK4 dataset). This setting is intended to test performance under clear data distribution shifts among nodes.
- *i.i.d. setting*, where a single dataset is randomly split and equally-distributed over multiple nodes. This setting evaluates how the approach scales with the number of nodes.

In all tasks and datasets, we employ 80% of the data to train both the privacy-preserving GAN and the classification model, while the remaining 20% of each dataset is used as test set. Test sets are balanced w.r.t. the label to avoid performance biases due to class imbalance.

B. Training procedure and metrics

1) *Decentralized distributed learning*: In all settings, we employ ResNet-18 [48] as classification model, trained by minimizing the cross-entropy loss with mini-batch gradient descent using the Adam optimizer. Mini-batch size is set to 32 and 8 for the Shenzhen and Montgomery datasets, respectively, and to 64 for skin lesion datasets. The learning rate is set to 10^{-4} . Data augmentation is carried out with random horizontal

flip; for skin images we additionally apply random 90-degree rotations. All images are resized to 256×256 .

The node federation is trained for T rounds. At each round of training, each node receives the model and a buffer of synthetic data from a randomly-chosen predecessor, fine-tunes the received model to its private data for E epochs, and sends the updated model and its own buffer of synthetic samples to a randomly-chosen successor. In our implementation, at each round nodes are randomly ordered to establish each node’s predecessor and successor: given our focus on medical applications, we can assume that the number of nodes is low enough that synchronization is not an issue. However, asynchronicity can be achieved by assuming that nodes can store incoming data in queue: if the distribution of successor nodes is uniform and computation times are similar for all nodes, this is on average equivalent to the synchronous case.

2) *GAN training*: The proposed privacy-preserving GAN uses StyleGAN2-ADA [49] as a backbone, because of its suitability in low-data regimes and its generation capabilities. Training is carried out in two steps: 1) the GAN is initially trained for 800,000 iterations without any privacy-preserving loss, to support learning of high-quality visual features; 2) we enable the privacy-preserving loss and fine-tune the mode for additional 150,000 iterations, in order to limit the embedding of patient-specific patterns in the GAN latent space. In our classification setting, GANs are trained in a label-conditioned fashion with a mini-batch size of 32 and learning rate 0.0025 for both the generator and the discriminator. We evaluate the generator’s capability to synthesize realistic images by means of the Fréchet Inception Distance (FID) [45]. In order to quantitatively evaluate privacy preservation, we generate, for each real image, its closest synthetic sample by means of latent space projection (described in Sect. IV-C.2), and compute the average LPIPS distance [23] between such pairs: a sufficiently high value implies the impossibility to reconstruct real images from the generator.

C. Results

1) *Distributed training*: We initially evaluate the performance (in terms of classification accuracy) of our approach, trained for 100 rounds with 100 epochs per round, in the *non-i.i.d.* setting, and compare its results to those achieved in case of a) non-distributed training of a single model on the union of the datasets, and b) centralized distributed learning where a central node receives a set of 256 privacy-preserving synthetic samples from each node and trains a global model. Classification accuracy is reported for each dataset: in distributed learning scenarios, performance is computed using the final model at the node where that dataset is located. From the results reported in Table I, two insights can be drawn: 1) on large datasets, as in the case of Shenzhen and all the melanoma datasets, our approach performs worse non-distributed training (as can be expected); 2) surprisingly, on smaller datasets such as Montgomery, our approach is able to outperform non-distributed training: a possible explanation lies in the data augmentation effect induced by the use of synthetic examples, which has been shown to reduce overfitting and help improve performance in low-data regimes [50].

TABLE I

COMPARISON BETWEEN THE PROPOSED APPROACH AND CENTRALIZED BASELINES. IN THE DISTRIBUTED LEARNING SETTING, RESULTS ARE OBTAINED WITH A BUFFER SIZE OF 512, 100 ROUNDS AND 100 EPOCHS PER ROUND.

Methods	Tuberculosis			Melanoma			
	Shenzhen	Montgomery	Avg.	BCN	HAM	MSK4	Avg.
Non-distributed training on dataset union	0.823	0.721	0.772	0.784	0.815	0.798	0.799
Centralized distributed learning with synthetic data	0.624	0.495	0.559	0.568	0.443	0.583	0.531
Decentralized distributed learning (ours)	0.712	0.772	0.742	0.776	0.765	0.656	0.732

TABLE II

ACCURACY CONVERGENCE AMONG FEDERATED NODE MODELS. RESULTS OBTAINED WITH A BUFFER SIZE OF 512.

Rounds	Epochs	Tuberculosis		Melanoma		
		Shenzhen	Montgomery	BCN	HAM	MSK4
10	1	0.544 ± 0.040	0.525 ± 0.042	0.614 ± 0.064	0.586 ± 0.082	0.603 ± 0.076
	10	0.665 ± 0.217	0.620 ± 0.145	0.673 ± 0.122	0.653 ± 0.166	0.636 ± 0.036
	100	0.670 ± 0.220	0.750 ± 0.173	0.724 ± 0.077	0.672 ± 0.143	0.657 ± 0.046
100	1	0.642 ± 0.155	0.631 ± 0.129	0.716 ± 0.059	0.659 ± 0.142	0.646 ± 0.046
	10	0.708 ± 0.170	0.772 ± 0.101	0.727 ± 0.083	0.710 ± 0.115	0.655 ± 0.043
	100	0.712 ± 0.127	0.772 ± 0.045	0.776 ± 0.049	0.765 ± 0.079	0.656 ± 0.033

We proceed to evaluate the agreement between models trained on each node, by measuring the standard deviation of the classification accuracy obtained by all nodes' models for each specific dataset, for different combinations of numbers of rounds and epochs per round. Table II shows that, in our default configuration with 100 rounds and 100 epochs per round, models tend to converge to similar predictions with limited variability, lower than 0.06 in four cases out of six. The performance on the Shenzhen (tuberculosis) dataset exhibits a larger variability, which can be explained by the lower generalization capabilities of the model trained on the very small Montgomery dataset.

A key component of the proposed architecture is the sharing of synthetic samples among all federated nodes. We evaluate the impact of the buffer size on classification performance, and compare with the case when the buffer is removed (i.e., only the model is shared). Results, evaluated on the tuberculosis task (which is the only one we use also for the subsequent evaluations on the architectural components) with 100 training rounds and different epochs per round, are reported in Table III and indicate that the experience replay strategy is necessary to allow the whole system to effectively learn with *non-i.i.d.* data. In general, the presence of larger buffer size ensures that common and robust features are learned, leading to significant performance improvements, especially on small datasets such as Montgomery with a performance gain of about 9 percent points between no buffer and a buffer size of 2048 samples. However, in all the experiments, we use buffer size of 512 as it represents the best compromise between accuracy and memory consumption on all the employed datasets.

We then evaluate the capability of the proposed method to scale with the size of the federated network, without losing effectiveness. We quantify this property in the *i.i.d.* setting on both tuberculosis (Shenzhen dataset) and skin lesion classification (BCN dataset) tasks, by equally splitting the available data on multiple nodes, and training for 100 rounds,

TABLE III

EFFECT OF BUFFER SIZE ON CLASSIFICATION ACCURACY.

Buffer Size	Epochs	Tuberculosis	
		Shenzhen	Montgomery
0	1	0.548 ± 0.081	0.526 ± 0.042
	10	0.667 ± 0.208	0.671 ± 0.160
	100	0.672 ± 0.197	0.705 ± 0.237
256	1	0.652 ± 0.176	0.666 ± 0.113
	10	0.674 ± 0.205	0.746 ± 0.095
	100	0.686 ± 0.157	0.757 ± 0.075
512	1	0.642 ± 0.155	0.631 ± 0.129
	10	0.708 ± 0.170	0.772 ± 0.101
	100	0.712 ± 0.127	0.772 ± 0.045
1024	1	0.663 ± 0.162	0.659 ± 0.111
	10	0.686 ± 0.196	0.752 ± 0.101
	100	0.704 ± 0.143	0.788 ± 0.049
2048	1	0.661 ± 0.174	0.685 ± 0.083
	10	0.694 ± 0.206	0.758 ± 0.104
	100	0.712 ± 0.123	0.794 ± 0.074

with 100 epochs per round. Fig 2 shows how the proposed approach is able to keep classification accuracy high (on the two datasets there is a performance drop less than 3 percent points from 2 to 8 nodes). A slight decrease in performance can be observed as the number of nodes increase, which can be explained by the lower size of the training set available for each node.

Finally, we compare our method with the FedAvg approach [24], which is a suitable baseline as it has been shown to perform generally better than decentralized methods [38], [40] and results are in Table IV in both *i.i.d.* and *non-i.i.d.* settings for the tuberculosis and melanoma classification tasks². Since centralized methods benefit from the global view of all models by the central node, FedAvg's performance is slightly better on the *non-i.i.d.* scenario (in this case, with

²Results for FedAvg were computed using the Intel OpenFL framework [51]

TABLE IV
COMPARISON BETWEEN OUR APPROACH AND FEDAVG [24].

	<i>Non-i.i.d.</i>		<i>i.i.d.</i>					
	Tuberculosis	Melanoma	Tuberculosis			Melanoma		
	2 Nodes	3 Nodes	2 Nodes	4 Nodes	8 Nodes	2 Nodes	4 Nodes	8 Nodes
FedAvg [24]	0.744	0.782	0.777	0.808	0.838	0.754	0.712	0.686
Ours	0.745	0.716	0.793	0.820	0.828	0.818	0.803	0.792

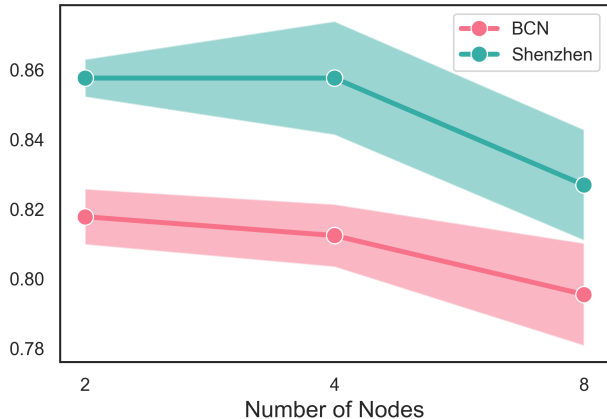


Fig. 2. Effect of the number of nodes on the proposed approach, in the *i.i.d.* setting (buffer size 256, 100 epochs, 100 rounds).

varying number of nodes), while, remarkably, our approach outperforms on average it on the *i.i.d.* settings, demonstrating better scalability capabilities. Considering all the obtained performance on the various scenarios, we can claim that our approach is at least on par with FedAvg, demonstrating that a principled feature integration approach may lead to better convergence properties over naïve parameter averaging even in a more complex case as the decentralized one.

2) *Privacy-preserving Data Synthesis*: After demonstrating the impact that the experience replay mechanism has on the proposed decentralized learning strategy, it is important to ensure that no sensitive information is leaving each node. Therefore, we quantify how much information of real samples is stored by our privacy-preserving method, and in particular in the mapping between latent space and synthetic images. To do so, we employ the projection method proposed in [16]: given a real image x , we find an intermediate latent point w such that the generated image $G(w)$ is most similar to x , by optimizing w to minimize the LPIPS distance [23] between x and $G(w)$.

In practice, for each image of the dataset used for GAN training, we perform backprojection to find its most similar synthetic sample, and measure the LPIPS distance between the original and projected images. Fig. 3 shows the histograms of the resulting distances on the Shenzhen dataset, using GAN models trained with and without the proposed privacy-preserving loss (both models start from the same w , for fairness). The histograms show that standard GAN training, with no privacy-preserving loss, tends to yield distances close to 0, demonstrating that real images are indeed encoded into the generator latent space; our model significantly mitigates

this issue, by synthesizing samples that are significantly more different than the original ones.

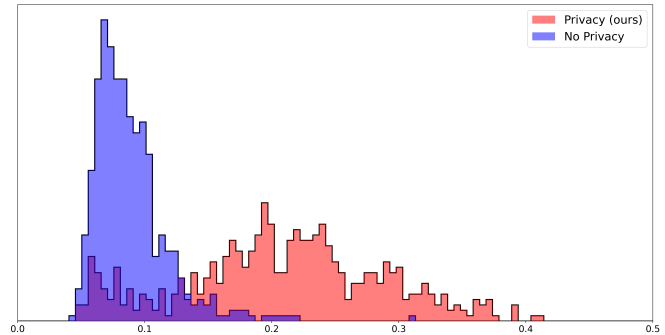


Fig. 3. **Quantitative analysis of privacy-preserving generation.** In blue, LPIPS distance histogram between real images and the corresponding images obtained through latent space projection using a GAN trained without the proposed privacy-preserving loss. In red, LPIPS distance histogram between real images and the closest images generated with the proposed approach.

In order to qualitatively substantiate these findings, Fig. 4 compares original samples from the Shenzhen dataset with the corresponding projections, generated with and without our privacy-preserving loss³. It is easy to notice that generated samples with a traditional GAN highly resemble real data, making it impossible to share such samples, albeit synthetic, in a privacy-safe manner, as they clearly contain patient information. Instead, comparing real images with the projections obtained from privacy-preserving GAN confirms the inability of the generator to find latent representations that recover real images used during training.

Given the high realism of generated samples, we run additional tests meant to push the level of privacy preservation: a) models are not shared among nodes — only synthetic buffers are sent and received (“*buffer-only sharing*”); b) models are trained only using synthetic data, even for the local dataset (“*synthetic-only training*”). Fig. 5 shows the internal architecture of each node in the two variants. Results obtained with these alternative privacy-enhanced strategies are provided in Table V, when training on the Shenzhen and Montgomery datasets in the *non-i.i.d.* setting for 100 rounds, with 100 epochs per round and a buffer size of 512. It can be noted that the “*buffer-only sharing*” variant achieves comparable performance to our standard setting, giving encouraging perspectives for further analysis. Instead, the “*synthetic-only training*” variant performs poorly, showing that using features

³We show only X-Ray synthesized samples as the effect is of our privacy-preserving strategy is more appreciable than in skin lesion data.

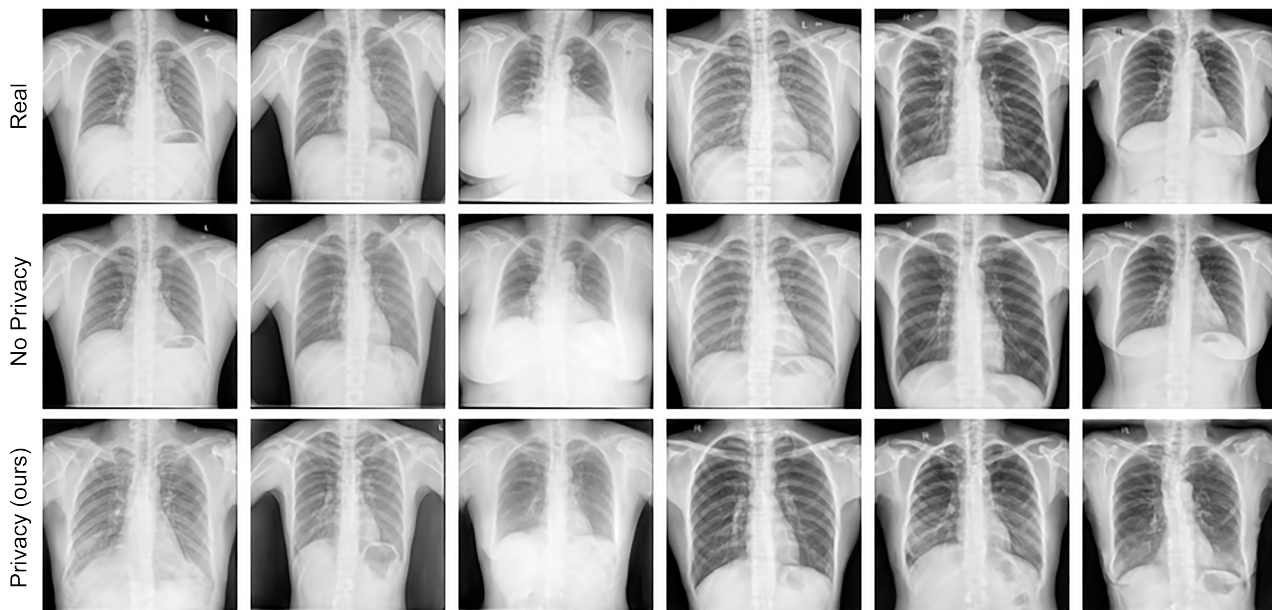


Fig. 4. Qualitative samples of our privacy-preserving generation. Top row: real images from the Shenzhen dataset. Middle row: projection with a standard GAN. Bottom row: projection with our privacy-preserving GAN.

TABLE V

CLASSIFICATION ACCURACY OF THE PROPOSED PRIVACY-ENHANCED STRATEGIES IN THE *non-i.i.d.* SETTING.

Configuration	Shenzhen	Montgomery
Standard	0.712	0.772
Buffer-only sharing	0.696	0.679
Synthetic-only training	0.585	0.517

from real images to train local models is essential to reach good global performance: nevertheless, further research on the generation process might lead to improvements in this aspect.

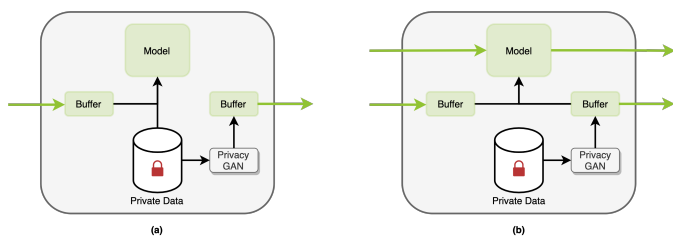


Fig. 5. Privacy-enhanced alternative architectures. (a) “Buffer-only sharing” configuration: a local node model is trained on real data, but only a buffer of synthetic samples is shared with other nodes. (b) “Synthetic-only training”: Even within the dataset owner node, models are trained on synthetic data only.

V. CONCLUSION

In this paper, we presented a novel decentralized distributed learning framework, that replaces traditional parameters averaging with a more principled feature integration approach based on the combination of experience replay and privacy-preserving generative models. In our approach, nodes communicate with each other by sharing local models and buffers of synthetic samples; local model updates are carried out in a way

that encourages the reuse and adaptation of features learned by other nodes, thus avoiding potentially disruptive effects due to blind feature averaging. Experimental results show that our method performs at least on par with state-of-the-art centralized approaches, and outperforms them in low-data availability scenarios, which is a typical setting in the medical domain. Additionally, quantitative and qualitative analysis shows that our privacy-preserving generation approach is able to synthesize samples that are significantly different from real data, while correctly supporting the learning of discriminative features. In the future, we aim at investigating some unexplored properties of our method: for instance, unlike all other existing methods based on parameter averaging is required, our approach does not strictly require that all nodes share the same model architecture. Model heterogeneity could therefore be employed to create a shared ensemble and combine different feature learning capabilities.

REFERENCES

- [1] J. Irvin, P. Rajpurkar, M. Ko, Y. Yu, S. Ciurea-Ilcus, C. Chute, H. Marklund, B. Haghighi, R. Ball, K. Shpanskaya *et al.*, “Chexpert: A large chest radiograph dataset with uncertainty labels and expert comparison,” in *Proceedings of the AAAI conference on artificial intelligence*, vol. 33, no. 01, 2019, pp. 590–597.
- [2] X. Wang, Y. Peng, L. Lu, Z. Lu, M. Bagheri, and R. M. Summers, “Chestx-ray8: Hospital-scale chest x-ray database and benchmarks on weakly-supervised classification and localization of common thorax diseases,” in *Proceedings of the IEEE conference on computer vision and pattern recognition*, 2017, pp. 2097–2106.
- [3] J. P. Cohen, P. Morrison, L. Dao, K. Roth, T. Q. Duong, and M. Ghassemi, “Covid-19 image data collection: Prospective predictions are the future,” *arXiv 2006.11988*, 2020. [Online]. Available: <https://github.com/ieee8023/covid-chestxray-dataset>
- [4] J. R. Zech, M. A. Badgeley, M. Liu, A. B. Costa, J. J. Titano, and E. K. Oermann, “Variable generalization performance of a deep learning model to detect pneumonia in chest radiographs: a cross-sectional study,” *PLoS medicine*, vol. 15, no. 11, p. e1002683, 2018.
- [5] Q. Yang, Y. Liu, T. Chen, and Y. Tong, “Federated machine learning: Concept and applications,” *ACM Transactions on Intelligent Systems and Technology (TIST)*, vol. 10, no. 2, pp. 1–19, 2019.

- [6] D. Evans, V. Kolesnikov, M. Rosulek *et al.*, “A pragmatic introduction to secure multi-party computation,” *Foundations and Trends in Privacy and Security*, vol. 2, no. 2-3, pp. 70–246, 2018.
- [7] L. Zhu, Z. Liu, and S. Han, “Deep leakage from gradients,” *Advances in Neural Information Processing Systems*, vol. 32, 2019.
- [8] J. Geiping, H. Bauermeister, H. Dröge, and M. Moeller, “Inverting gradients-how easy is it to break privacy in federated learning?” *Advances in Neural Information Processing Systems*, vol. 33, pp. 16937–16947, 2020.
- [9] B. Zhao, K. R. Mopuri, and H. Bilen, “idlg: Improved deep leakage from gradients,” *arXiv preprint arXiv:2001.02610*, 2020.
- [10] R. Ratcliff, “Connectionist models of recognition memory: constraints imposed by learning and forgetting functions,” *Psychological review*, vol. 97, no. 2, p. 285, 1990.
- [11] A. Robins, “Catastrophic forgetting, rehearsal and pseudorehearsal,” *Connection Science*, vol. 7, no. 2, pp. 123–146, 1995.
- [12] D. Rolnick, A. Ahuja, J. Schwarz, T. Lillicrap, and G. Wayne, “Experience replay for continual learning,” *Advances in Neural Information Processing Systems*, vol. 32, 2019.
- [13] P. Buzzega, M. Boschini, A. Porrello, D. Abati, and S. Calderara, “Dark experience for general continual learning: a strong, simple baseline,” *Advances in neural information processing systems*, vol. 33, pp. 15920–15930, 2020.
- [14] I. Goodfellow, J. Pouget-Abadie, M. Mirza, B. Xu, D. Warde-Farley, S. Ozair, A. Courville, and Y. Bengio, “Generative adversarial nets,” *Advances in neural information processing systems*, vol. 27, 2014.
- [15] M. Mirza and S. Osindero, “Conditional generative adversarial nets,” *arXiv preprint arXiv:1411.1784*, 2014.
- [16] T. Karras, S. Laine, M. Aittala, J. Hellsten, J. Lehtinen, and T. Aila, “Analyzing and improving the image quality of stylegan,” in *Proceedings of the IEEE/CVF conference on computer vision and pattern recognition*, 2020, pp. 8110–8119.
- [17] S. Candemir, S. Jaeger, K. Palaniappan, J. P. Musco, R. K. Singh, Z. Xue, A. Karargyris, S. Antani, G. Thoma, and C. J. McDonald, “Lung segmentation in chest radiographs using anatomical atlases with nonrigid registration,” *IEEE transactions on medical imaging*, vol. 33, no. 2, pp. 577–590, 2013.
- [18] S. Jaeger, S. Candemir, S. Antani, Y.-X. J. Wang, P.-X. Lu, and G. Thoma, “Two public chest x-ray datasets for computer-aided screening of pulmonary diseases,” *Quantitative imaging in medicine and surgery*, vol. 4, no. 6, p. 475, 2014.
- [19] S. Jaeger, A. Karargyris, S. Candemir, L. Folio, J. Siegelman, F. Callaghan, Z. Xue, K. Palaniappan, R. K. Singh, S. Antani *et al.*, “Automatic tuberculosis screening using chest radiographs,” *IEEE transactions on medical imaging*, vol. 33, no. 2, pp. 233–245, 2013.
- [20] M. Combalia, N. C. Codella, V. Rotemberg, B. Helba, V. Vilaplana, O. Reiter, C. Carrera, A. Barreiro, A. C. Halpern, S. Puig *et al.*, “Bcn20000: Dermoscopic lesions in the wild,” *arXiv preprint arXiv:1908.02288*, 2019.
- [21] P. Tschandl, C. Rosendahl, and H. Kittler, “The ham10000 dataset, a large collection of multi-source dermatoscopic images of common pigmented skin lesions,” *Scientific data*, vol. 5, no. 1, pp. 1–9, 2018.
- [22] N. C. Codella, D. Gutman, M. E. Celebi, B. Helba, M. A. Marchetti, S. W. Dusza, A. Kalloo, K. Liopyris, N. Mishra, H. Kittler *et al.*, “Skin lesion analysis toward melanoma detection: A challenge at the 2017 international symposium on biomedical imaging (isbi),” in *IEEE international symposium on biomedical imaging (ISBI 2018)*. IEEE, 2018, pp. 168–172.
- [23] R. Zhang, P. Isola, A. A. Efros, E. Shechtman, and O. Wang, “The unreasonable effectiveness of deep features as a perceptual metric,” in *Proceedings of the IEEE conference on computer vision and pattern recognition*, 2018, pp. 586–595.
- [24] B. McMahan, E. Moore, D. Ramage, S. Hampson, and B. A. y Arcas, “Communication-efficient learning of deep networks from decentralized data,” in *Artificial intelligence and statistics*. PMLR, 2017, pp. 1273–1282.
- [25] W. Li, F. Milletari, D. Xu, N. Rieke, J. Hancox, W. Zhu, M. Baust, Y. Cheng, S. Ourselin, M. J. Cardoso *et al.*, “Privacy-preserving federated brain tumour segmentation,” in *International workshop on machine learning in medical imaging*. Springer, 2019, pp. 133–141.
- [26] A. G. Roy, S. Siddiqui, S. Pölsterl, N. Navab, and C. Wachinger, “Braitorrent: A peer-to-peer environment for decentralized federated learning,” *arXiv preprint arXiv:1905.06731*, 2019.
- [27] I. Dayan, H. R. Roth, A. Zhong, A. Harouni, A. Gentili, A. Z. Abidin, A. Liu, A. B. Costa, B. J. Wood, C.-S. Tsai *et al.*, “Federated learning for predicting clinical outcomes in patients with covid-19,” *Nature medicine*, vol. 27, no. 10, pp. 1735–1743, 2021.
- [28] I. Feki, S. Ammar, Y. Kessentini, and K. Muhammad, “Federated learning for covid-19 screening from chest x-ray images,” *Applied Soft Computing*, vol. 106, p. 107330, 2021.
- [29] J. Pang, Y. Huang, Z. Xie, J. Li, and Z. Cai, “Collaborative city digital twin for the covid-19 pandemic: A federated learning solution,” *Tsinghua science and technology*, vol. 26, no. 5, pp. 759–771, 2021.
- [30] T. Li, A. K. Sahu, M. Zaheer, M. Sanjabi, A. Talwalkar, and V. Smith, “Federated optimization in heterogeneous networks,” *Proceedings of Machine Learning and Systems*, vol. 2, pp. 429–450, 2020.
- [31] P. Kairouz, H. B. McMahan, B. Avent, A. Bellet, M. Bennis, A. N. Bhagoji, K. Bonawitz, Z. Charles, G. Cormode, R. Cummings *et al.*, “Advances and open problems in federated learning,” *Foundations and Trends in Machine Learning*, vol. 14, no. 1–2, pp. 1–210, 2021.
- [32] I. J. Goodfellow, M. Mirza, D. Xiao, A. Courville, and Y. Bengio, “An empirical investigation of catastrophic forgetting in gradient-based neural networks,” *arXiv preprint arXiv:1312.6211*, 2013.
- [33] N. Shoham, T. Avidor, A. Keren, N. Israel, D. Benditkis, L. Mor-Yosef, and I. Zeitak, “Overcoming forgetting in federated learning on non-iid data,” *arXiv preprint arXiv:1910.07796*, 2019.
- [34] H. Wang, M. Yurochkin, Y. Sun, D. Papailiopoulos, and Y. Khazaeni, “Federated learning with matched averaging,” *arXiv preprint arXiv:2002.06440*, 2020.
- [35] L. Xie, K. Lin, S. Wang, F. Wang, and J. Zhou, “Differentially private generative adversarial network,” *arXiv preprint arXiv:1802.06739*, 2018.
- [36] X. Lian, C. Zhang, H. Zhang, C.-J. Hsieh, W. Zhang, and J. Liu, “Can decentralized algorithms outperform centralized algorithms? a case study for decentralized parallel stochastic gradient descent,” *Advances in Neural Information Processing Systems*, vol. 30, 2017.
- [37] P. Vanhaesebrouck, A. Bellet, and M. Tommasi, “Decentralized collaborative learning of personalized models over networks,” in *Artificial Intelligence and Statistics*. PMLR, 2017, pp. 509–517.
- [38] A. Lalitha, O. C. Kilinc, T. Javidi, and F. Koushanfar, “Peer-to-peer federated learning on graphs,” *arXiv preprint arXiv:1901.11173*, 2019.
- [39] T. Wink and Z. Nochta, “An approach for peer-to-peer federated learning,” in *2021 51st Annual IEEE/IFIP International Conference on Dependable Systems and Networks Workshops (DSN-W)*. IEEE, 2021, pp. 150–157.
- [40] T. Sun, D. Li, and B. Wang, “Decentralized federated averaging,” *arXiv preprint arXiv:2104.11375*, 2021.
- [41] D. Chen, T. Orekondy, and M. Fritz, “Gs-wgan: A gradient-sanitized approach for learning differentially private generators,” *Advances in Neural Information Processing Systems*, vol. 33, pp. 12673–12684, 2020.
- [42] J. Song and J. C. Ye, “Federated cyclegan for privacy-preserving image-to-image translation,” *arXiv preprint arXiv:2106.09246*, 2021.
- [43] L. Zhang, B. Shen, A. Barnawi, S. Xi, N. Kumar, and Y. Wu, “FeddpGAN: federated differentially private generative adversarial networks framework for the detection of covid-19 pneumonia,” *Information Systems Frontiers*, vol. 23, no. 6, pp. 1403–1415, 2021.
- [44] K. Simonyan and A. Zisserman, “Very deep convolutional networks for large-scale image recognition,” in *3rd International Conference on Learning Representations, ICLR 2015, San Diego, CA, USA, May 7-9, 2015, Conference Track Proceedings*, 2015.
- [45] M. Heusel, H. Ramsauer, T. Unterthiner, B. Nessler, and S. Hochreiter, “Gans trained by a two time-scale update rule converge to a local nash equilibrium,” *Advances in neural information processing systems*, vol. 30, 2017.
- [46] M. Delange, R. Aljundi, M. Masana, S. Parisot, X. Jia, A. Leonardis, G. Slabaugh, and T. Tuytelaars, “A continual learning survey: Defying forgetting in classification tasks,” *IEEE Transactions on Pattern Analysis and Machine Intelligence*, 2021.
- [47] M. Riemer, I. Cases, R. Ajemian, M. Liu, I. Rish, Y. Tu, and G. Tesauro, “Learning to learn without forgetting by maximizing transfer and minimizing interference,” *arXiv preprint arXiv:1810.11910*, 2018.
- [48] K. He, X. Zhang, S. Ren, and J. Sun, “Deep residual learning for image recognition,” in *Proceedings of the IEEE conference on computer vision and pattern recognition*, 2016, pp. 770–778.
- [49] T. Karras, M. Aittala, J. Hellsten, S. Laine, J. Lehtinen, and T. Aila, “Training generative adversarial networks with limited data,” in *NeurIPS*, vol. 33, 2020, pp. 12104–12114.
- [50] M. Pennisi, S. Palazzo, and C. Spampinato, “Self-improving classification performance through GAN distillation,” in *ICCVW*, 2021, pp. 1640–1648.
- [51] G. A. Reina, A. Gruzdev, P. Foley, O. Perepelkina, M. Sharma, I. Davidiyuk, I. Trushkin, M. Radionov, A. Mokrov, D. Agapov *et al.*, “Openfl: An open-source framework for federated learning,” *arXiv preprint arXiv:2105.06413*, 2021.